Geophysical Research Letters

RESEARCH LETTER
10.1029/2021GL095678

Urbanization Amplifies Nighttime Heat Stress on Warmer Days Over the US

Chandan Sarangi[1,2,3], Yun Qian[3], Jianfeng Li[3], L. Ruby Leung[3], T. C. Chakraborty[3,4], and Ying Liu[3]

[1]Indian Institute of Technology, Chennai, India, [2]Laboratory of Atmospheric and Climate Sciences, IIT Madras, Chennai, India, [3]Pacific Northwest National Laboratory, Richland, WA, USA, [4]School of the Environment, Yale University, New Haven, CT, USA

Key Points:

- Multiyear cloud resolving simulations are done to understand the thermodynamical constrains of urban-induced heat stress
- While urban-induced temperature increase peaks during nighttime, the associated moisture reduction is maximum during daytime
- Heat related human discomfort exposure increases by 3–5 hr day^{-1} due to urbanization

Supporting Information:

Supporting Information may be found in the online version of this article.

Correspondence to:

C. Sarangi and Y. Qian,
chandansarangi@civil.iitm.ac.in;
yun.qian@pnnl.gov

Citation:

Sarangi, C., Qian, Y., Li, J., Leung, L. R., Chakraborty, T. C., & Liu, Y. (2021). Urbanization amplifies nighttime heat stress on warmer days over the US. *Geophysical Research Letters*, *48*, e2021GL095678. https://doi.org/10.1029/2021GL095678

Received 26 AUG 2021
Accepted 30 NOV 2021

Author Contributions:

Conceptualization: Chandan Sarangi, Yun Qian, L. Ruby Leung
Data curation: Chandan Sarangi, T. C. Chakraborty, Ying Liu
Formal analysis: Chandan Sarangi, Jianfeng Li, T. C. Chakraborty
Funding acquisition: Yun Qian, L. Ruby Leung
Project Administration: Yun Qian
Writing – original draft: Chandan Sarangi
Writing – review & editing: Yun Qian, Jianfeng Li, L. Ruby Leung, T. C. Chakraborty, Ying Liu

Abstract The impact of heat on human health is well-recognized, with excess heat stress in urban areas (urban heat stress intensity, UHSI) adversely affecting rapidly growing urban populations. However, the physical associations of UHSI with urban heat island (UHI), urban-induced change in moisture (UQI) and background temperature are not well understood. Multi-year convection-permitting simulations over the US show that UHI effect peaks during nighttime (2–5°C) but maximum UQI occurs in daytime (0.01–2 g kg^{-1}), resulting in competing effects on UHSI. UHI dynamics dominate the diurnal variations in UHSI with intensified urban-induced human discomfort during nighttime (3–5 hr day^{-1}). UHSI is very sensitive to the background temperature, especially over the southeastern US, with distinct nighttime UHSI amplification of ∼0.5 hr day^{-1} degree^{-1} rise in the background temperature. Spatial variability of UHSI is also dominated by the UHI with possible constrains from background moisture availability.

Plain Language Summary While urbanization increases the temperature of urban regions compared to rural regions, it also decreases the moisture in the urban air. Thus, urbanization can have heterogeneous effect on heat stress (a net effect of ambient temperature and moisture) on warmer days. In this study, we employed convection-permitting simulations for six consecutive summer seasons over the US to examine the spatiotemporal variability of urban-induced heat stress and its variation on relatively warmer days. We show that the heat stress is distinctly greater over the urban regions compared to surrounding rural regions in Eastern US and specifically over southeastern US. Moreover, this urban effect on heat stress grows stronger on warmer periods, specifically during nighttime, while the association can be opposite during daytime due to the dominant moisture effect. Quantitatively, urbanization can increase heat caution hours by 3–5 hr day^{-1} and its sensitivity to background temperature is ∼0.5 hr day^{-1} degree^{-1} over many US cities.

1. Introduction

Urbanization is the most tangible local-scale impact of humans on the Earth's surface and the surface climate (Jia et al., 2020; Kalnay & Cai, 2003). Urbanization-associated perturbations in land use/land cover (LULC) can substantially alter the micro-climate of cities via re-adjustment of the surface energy balance. Specifically, urban regions are observed to be warmer (based on temperature measured at 2 meter) and drier (based on moisture mixing ratio at 2 meter) than peripheral rural areas, commonly referred in the literature as Urban Heat Island (UHI) (e.g., Oke and Cleugh., 1991) and Urban Dry Island (UQI) (Oke & Cleugh, 1987), respectively. Along with LULC changes, urbanization is also associated with increases in the heat generated by anthropogenic activities or anthropogenic heat flux (AHF) into the urban atmosphere. Notably, the global urban population has crossed ∼4 billion (half of the total global population) and is expected to reach up to ∼7 billion, accounting for two-third of the total global population, by 2050 (Ritchie & Max, 2018). The human body's ability to dissipate metabolic heat through evaporative cooling (sweating) and heat conduction is inversely proportional to the ambient temperature and humidity (Sherwood & Huber, 2010). Consequently, urbanization-induced perturbations in micro-climate can substantially affect a large portion of the global population in the near future via urban-induced heat stress intensity (UHSI) and its associated economic impacts (Estrada et al., 2017; Frumkin, 2002; Laaidi et al., 2012; Tan et al., 2010).

Previous modeling studies concluded that background warming under heatwaves amplify the urban-rural temperature differences (Wouters et al., 2017). While such findings were corroborated by nearby weather station

observations, these studies mostly analyzed single events for single cities such as Baltimore (Li & Bou-Zeid, 2013; Li & Bou-Zeid, 2014; Li et al., 2015) and New York (Li et al., 2015; Ramamurthy & Bou-Zeid, 2017; Schatz & Kucharik, 2015; Tewari et al., 2019); so how generalizable those results are is not clear. Recently, Zhao et al. (2018) found that UHI enhancement during heatwave conditions is significant and distinct over Eastern US (EUS). However, they used coarsely resolved offline land surface model (LSM) simulations in their study. Using observational data over 54 US cities, Scott et al. (2018) found that the UHI intensity tends to decrease with increasing temperature in many US cities, while a few studies reported no synergistic associations between UHI and high temperature days over cities like Philadelphia (Ramamurthy & Bou-Zeid, 2017), Oklahoma City (Basara et al., 2008) and Singapore (Chew et al., 2021). Thus, the sensitivity of UHI to background temperature (T) is still highly uncertain.

In line with the concept of urban heat island intensity (Katavoutas & Founda, 2019) introduced the term UHSI (Urban Heat Stress Intensity) and compared bioclimatic indices between urban and non-urban sites during heatwave and non-heatwave periods to demonstrate potential associations between heatwaves and the UHSI. However, our understanding of the sensitivity of UHSI to ambient temperature rise is limited. Changes from rural to urban surface cover have both temperature (UHI) and moisture (UQI) effects, which can be closely coupled. Increase in temperature induces vapor pressure deficit and reduces evapotranspiration at the urban core, thereby increasing the urban-induced dryness or UQI (Hao et al., 2018). Similarly, UQI intensification may reduce cloud formation over the urban core (relative to rural regions), thus increasing the UHI (Du et al., 2019). However, UHI and UQI have competing effects on UHSI. Keeping all other factors constant, heat stress increases with increasing UHI values but decreases with increasing UQI values (Fischer et al., 2012). Therefore, urban-induced drying can offset the heat stress enhancement due to UHI (Wang & Gong, 2010; Yang et al., 2019). Notably, urban-rural differences in vegetation type and background climate can also affect UHI and UQI intensities (Chakraborty et al., 2017; Manoli et al., 2020; Zhao et al., 2018).

In 2020, ∼83% of the total population in the US lived in cities and urban areas. The larger of these cities are mostly concentrated over EUS (east of 105°W). Here, using a high-resolution convection-permitting regional modeling framework and satellite data, we investigate the spatiotemporal characteristics of UHSI and examine its sensitivity to background temperature in this region. Further, we illustrate the relative role of UHI and UQI on UHSI and UHSI-T associations.

2. Model Setup and Numerical Experiments

The Weather Research and Forecasting (WRF) model Version 3.8.1 (Skamarock & Klemp, 2008) was used to perform high resolution simulations, with the model domain (approximate 23.3°N–48.9°N and 66.2°W–108.2°W) centered on EUS (Figure S1 in Supporting Information S1). A single domain with 799 × 685 grid points is configured at convection-permitting scale of 4 km resolution with 64 vertical layers (approximately 90 m vertical resolution near the surface). Initial and boundary conditions, including sea surface temperature, are derived from North American Regional Reanalysis https://www.ncdc.noaa.gov/data-access/model-data/model-datasets/north-american-regional-reanalysis-narr data (Mesinger et al., 2006). Data nudging or assimilation was not applied. The Noah LSM (Chen & Dudhia, 2001), coupled with a singer-layer urban canopy model (Kusaka et al., 2001) (Kusaka & Kimura, 2004), was used to represent land surface processes. Additional model physics include the Thompson microphysics scheme (Thompson et al., 2008), the Rapid Radiative Transfer Model for longwave radiation (Mlawer et al., 1997), the Goddard shortwave radiation scheme (Chou & Suarez, 1994), the Mellor-Yamada-Janjić (Janjić (2001) planetary boundary layer scheme, and the Eta surface layer scheme (Janjić, 1994, 2001).

Accurate simulations of urban-induced micro-meteorological perturbations require accurate urban land classifications and AHF emissions. Traditionally, the default Moderate Resolution Imaging Spectroradiometer (MODIS)-based LULC types are used in the Noah land surface module. We modified the Noah module to add three more urban LULC subcategories: commercial, high-intensity residential, and low-intensity residential (Chen et al., 2014; Yang et al., 2019) to capture more realistically the variability in urban characteristics in EUS. Further, the LSM was modified to add AHF directly to the sensible heat flux term in the LSM to represent the dynamic AHF in the simulation using the spatially heterogeneous global data set from (Lee et al., 2014).

Two experiments were performed with the above physics schemes. The control simulation (CNTL) incorporates the urbanization effect with realistic urban land use and AHF. The sensitivity experiment (NO_URB) is identical to the CNTL experiment except that urban grids are replaced by the dominant land cover type in the background/nearby rural grids, and AHF is not considered. Both experiments were conducted for six consecutive spring-summer seasons (April–August: 2008–2013). As our study focuses on summertime urban heat stress, we only analyze and present results of June-July-August (JJA) in each year.

Urbanization effect on UHI and UQI is estimated from the difference of 2-m temperature and water vapor mixing ratio, respectively, between CNTL and NO_URB runs. The enhancement in thermal discomfort due to urbanization is calculated using a heat index, HI (Steadman, 1971), which is defined as

$$\begin{aligned} HI = &-42.379 + 2.04901523T_F + 10.14333127RH - 0.22475541T_F RH - 6.83783 \\ &\times 10^{-3}T_F^2 - 5.481717 \times 10^{-2}RH^2 + 1.22874 \times 10^{-3}T_F^2 RH + 8.5282 \\ &\times 10^{-4}T_F RH^2 - 1.99 \times 10^{-6}T_F^2 RH^2 \end{aligned} \quad (1)$$

where, T_F and RH denote air temperature (in degrees Fahrenheit) and relative humidity (in %), respectively. Note that we use RH instead of specific humidity in Equation 1, as per the technical definition of HI (https://www.wpc.ncep.noaa.gov/html/heatindex_equation.shtml). The difference in 2-m HI between CNTL and NO_URB provides an estimate of UHSI due to urbanization (Equation 2). Generally, HI is used as a metric to classify heat extreme scenarios. Specifically, HI of 27–32°C is flagged as "heat caution" as fatigue and cramps can develop due to extended exposure. Similarly, HI of 32–41°C is flagged as "heat extreme period" as such exposure can even lead to heat stroke. Finally, HI ≥ 42°C is flagged as "danger and extreme danger" as heat stroke becomes probable and imminent. Conservatively, Heat caution hours (HCH) in a day (i.e., number of hours when HI ≥ 27°C) is used for our analysis. Similar to Equation 2, the difference in the number of heat caution hours (ΔHCH) is used in our study to denote the increased exposure time of humans to potential UHSI (Equation 3). Further, the separate contributions of urban-induced changes in Temperature and moisture on the enhancement in HCH are calculated using Equations 4 and 5, respectively.

$$\mathrm{UHSI} = \mathrm{HI_{CNTL}} - \mathrm{HI_{No\_URB}} \quad (2)$$

$$\Delta\mathrm{HCH} = \mathrm{HCH_{CNTL}} - \mathrm{HCH_{No\_URB}} \quad (3)$$

$$\Delta\mathrm{HCH(T)} = \mathrm{HCH(T_{F\,CNTL}, RH_{CNTL})} - \mathrm{HCH(T_{FNo\_URB}, RH_{CNTL})} \quad (4)$$

$$\Delta\mathrm{HCH(RH)} = \mathrm{HCH(T_{F\,CNTL}, RH_{CNTL})} - \mathrm{HCH(T_{F\,CNTL}, RH_{No\_URB})} \quad (5)$$

3. Model Evaluation at City Scale

The model simulated UHI values at surface ($\mathrm{UHI_{surface}}$) are first evaluated against satellite-derived estimates of mean summer (JJA) $\mathrm{UHI_{surface}}$ from MODIS overpasses (4 times a day). To calculate $\mathrm{UHI_{surface}}$ from MODIS, the mean Land Surface Temperature (LST) over the city is subtracted from the mean LST of a normalized buffered region (which is approximately equal to the area of the city) around the city (see Chakraborty et al., 2021). For consistency, corresponding $\mathrm{UHI_{surface}}$ values are calculated using the same methodology for the WRF CNTL run and averaged over the 6-year simulation period.

The simulated daily mean summer $\mathrm{UHI_{surface}}$ compares well with observed values over most of the cities in southern half of EUS (Latitudes < 37°N) with magnitudes ~0.5–3.5°C (Figures 1a and 1b). The $\mathrm{UHI_{surface}}$ over northern half of EUS ranges between ~1.5 and ~4°C in the satellite observation. In comparison, the simulated $\mathrm{UHI_{surface}}$ mostly ranges between ~2.5 to and ~4.5°C over northern EUS. In general, the simulated $\mathrm{UHI_{surface}}$ over some big cities are overestimated compared to satellite observations. For example, the MODIS-derived mean $\mathrm{UHI_{surface}}$ over New York and Atlanta is ~1.5°C lower than the corresponding simulated mean values. Note that satellite observations have missing data and uncertainties under partially cloudy conditions, which may induce biases to this evaluation (Chakraborty et al., 2020). However, the spatial pattern in daily mean $\mathrm{UHI_{surface}}$ over EUS is well captured by the simulation. The $\mathrm{UHI_{surface}}$ generally decreases from northeast to southwest of the EUS domain in both observations and the simulation.

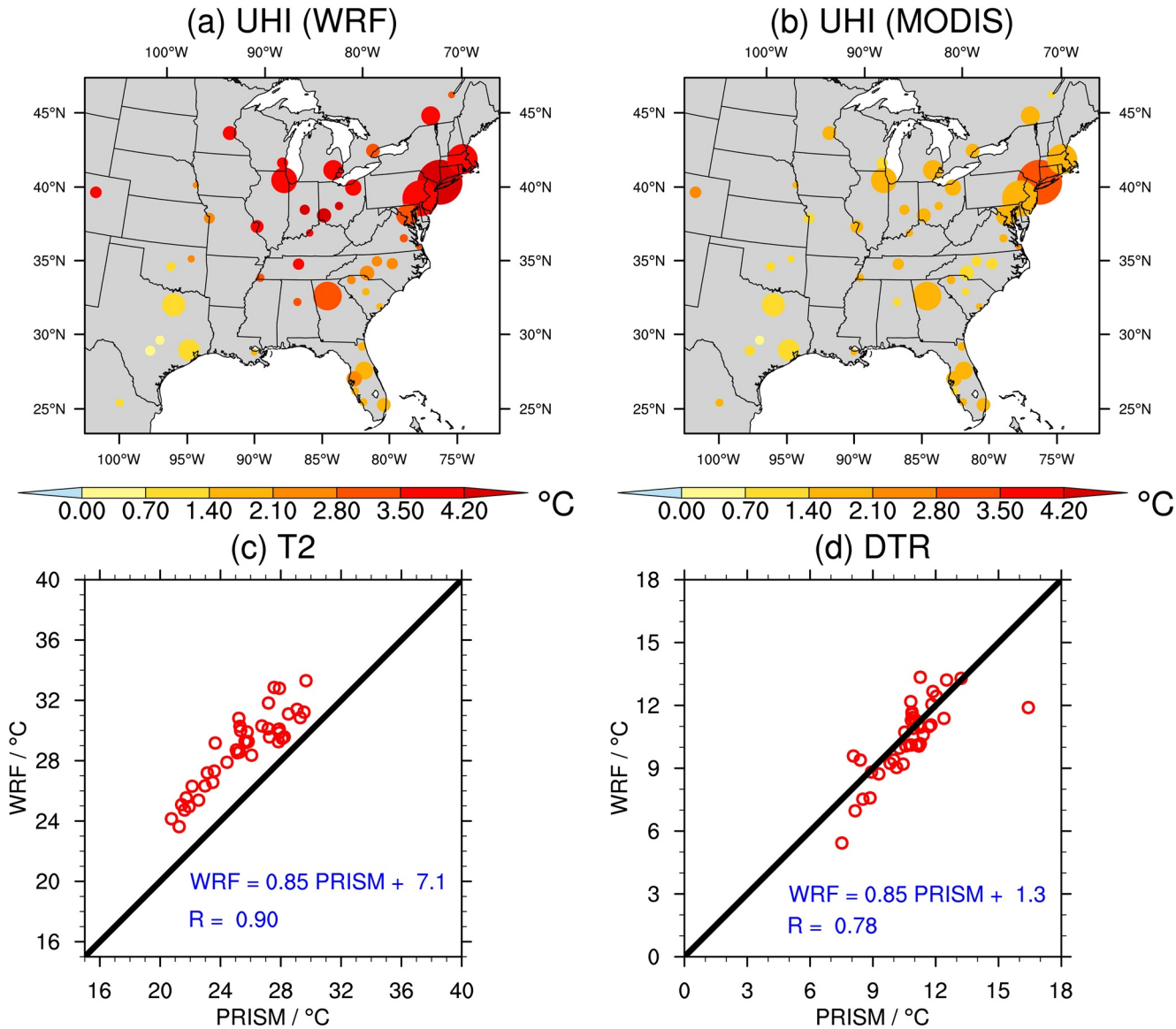

Figure 1. Panel a shows the 6-year summer June-July-August (JJA) mean values of CNTL-simulated $UHI_{surface}$ over city clusters of Eastern US (EUS). City clusters are defined as continuous nightlight-informed urban grids defined in the CNTL experiment and the size of the filled circles represents the population in city clusters. The temperature values over all the urban grids in a city (as shown in Figure S1 in Supporting Information S1) are averaged to report the city specific value. Panel b is the same as panel a, but for the corresponding 6-year summer mean values of Moderate Resolution Imaging Spectroradiometer derived $UHI_{surface}$. Panel c compares the Weather Research and Forecasting-simulated 6-year summer (JJA) mean values of daily mean air temperature (T2) with collocated observed values from PRISM (Parameter-elevation Relationships on Independent Slopes Model) data set using scatterplot. Panel d is the same as Panel c, but for the diurnal temperature range over city clusters of EUS.

The simulated daily mean 2-m temperature (Figure 1c) and diurnal temperature range (DTR) (Figure 1d) for each city, calculated as the difference between midday (1100–1400 LTC) and midnight (2100–0200 LTC) values based on hourly data from CNTL, are evaluated using correlation coefficients (R) against corresponding PRISM observations (Daly et al., 2007). During summer, the mean daily temperature varies between ~24 and ~35°C in EUS cities. There is a good correspondence between the simulation and PRISM data ($R = 0.9$), but biases of ~2–3°C are obvious, similar to biases (~2°C) found in other studies using WRF (Li & Bou-Zeid, 2014; Tewari et al., 2019). Warm and dry biases over central and eastern US have been longstanding and well-documented issues in weather and climate models (Lin et al., 2017; Ma et al., 2018; Morcrette et al., 2018; Qian et al., 2020). Since, these large-scale biases are present in both CNTL and NO_URB, their effect on modeling UHI, UQI, and UHSI should be negligible.

Comparison of the simulated and observed DTR shows that the mean thermal climate is well-reproduced at city scale (R ~0.8 and very low biases). Further, ability of the model to reproduce the daily variability over each city is evaluated between the modeled and observed daily air temperature values over each city (Figure S2a in Supporting Information S1). Similar analysis is also presented for the daily minimum and maximum temperatures, separately (Figures S2b–S2c in Supporting Information S1). Note that both city-scale minimum and maximum temperatures are overestimated by the CNTL runs over EUS (Figure not shown), resulting in negligible differences between simulated and observed DTR. Overall, the model satisfactorily reproduces the daily variability of near surface thermal environment (R ~0.6–0.8), irrespective of the location of the city. Comparison of the daily variability of simulated RH against that of ERA reanalysis also shows reasonable agreement (R ~0.7) (Figure S2d in Supporting Information S1). Further, the ERA5-Land reanalysis-based HI is computed and compared against the daily mean HI in the CNTL simulation over the cities in EUS (Figure S3 in Supporting Information S1). It can be seen that the spatio-temporal variability of the simulated HI matches quite well ($R > 0.7$) with the reanalysis product for most of the EUS cities. However, a small offset is present in magnitude which could be attributed to the discrepancy in urban representation and resolution (with ERA5-Land being coarser) between the two data sets. In summary, despite biases in the simulated values, the model captures the spatio-temporal variability of temperature, moisture and heat index reasonably well.

4. Daytime Versus Nighttime UHI, UQI and UHSI

Figures 2a and 2b show the midday and midnight UHI over urban clusters averaged from hourly simulated data over 6 summer seasons. Different scales are used in plotting the changes at midday versus midnight to display the spatial variability more clearly. As expected, LULC change from background to urban and AHF lead to a warmer environments. However, changes in the magnitude of UHI between day and night are distinct. While the summer mean nighttime UHI over EUS cities ranges from 1.6°C to 4.8°C, the mean daytime UHI has a much smaller range between −0.7°C and 1.4°C. However, the region influenced by UHI is greater (radius ~100–200 km from city center in northern cities) during the turbulent daytime compared to nighttime (not shown). The simulated changes in midday and midnight UQI are shown in Figures 2c and 2d. In general, urbanization reduces moisture regardless of the time of day. However, in contrast to the diurnal pattern of UHI, the daytime urban-induced dryness (negative UQI values) is greater than nighttime over all cities. During midday, the mean dryness at city cores ranges from 0.0 to 2.1 g kg^{-1}, but at night, the values are less than 0.8 g kg^{1}.

During daytime, the net radiation, and thus the available energy at the surface (which is dissipated as latent heat + sensible heat), is much greater than at night. Changing the natural surface cover to urban changes the partitioning of the surface available energy, as latent heat flux is reduced drastically with reduction in vegetation cover. As latent heat release is negligible during nighttime (Figures S4a–S4b in Supporting Information S1), the greater magnitude of UQI in daytime compared to nighttime is expected. Consequently, with urban land cover, a larger fraction of available energy at the surface is partitioned into sensible heat flux and ground heat storage. The enhancement in sensible heat triggers the UHI during daytime (Figures S4c–S4d in Supporting Information S1), but the enhancement in ground heat storage increases the heat emission at night and is the cause of the UHI peaking at nighttime (Varquez & Kanda, 2018). This thermal inertia of storing daytime heat and releasing it slowly during nighttime also enhances the daily minimum temperature (Varquez & Kanda, 2018). Although the enhancement in daily maximum temperature (during daytime) due to urbanization is also evident, many confounding factors such as turbulence and boundary layer convection reduce its magnitude compared to the nighttime UHI. Thus, urbanization also causes a distinct decrease in the DTR over all the cities (Figure S4e in Supporting Information S1).

Spatial heterogeneity in the UHI and UQI magnitudes over EUS is evident irrespective of the time of the day. While variability in the size of cities is indicated by the size of the circles in Figure 2, it appears that the magnitude of the UHI and UQI is a stronger function of the geographical location rather than the city size. In short, from northeastern US to southwestern or southeastern US, the UHI and UQI values change more obviously while within a region, there is less variability in the UHI and UQI despite the large variability in the city size. This indicates a role of the background climate/solar radiation. For quantification, we divide our study area into three sub-regions, namely Northern EUS (hereafter EUS_{North}), Southwestern EUS (EUS_{SW}) and Southeastern EUS (EUS_{SE}) and analyzed them separately (Table S1 and Figure S5 in Supporting Information S1). These regions closely follow the background climate zones. Magnitudes of the UHI and UQI are greatest over EUS_{North}, followed by EUS_{SW} and EUS_{SE}. This is mainly because latent heat reduction and sensible heat enhancement are

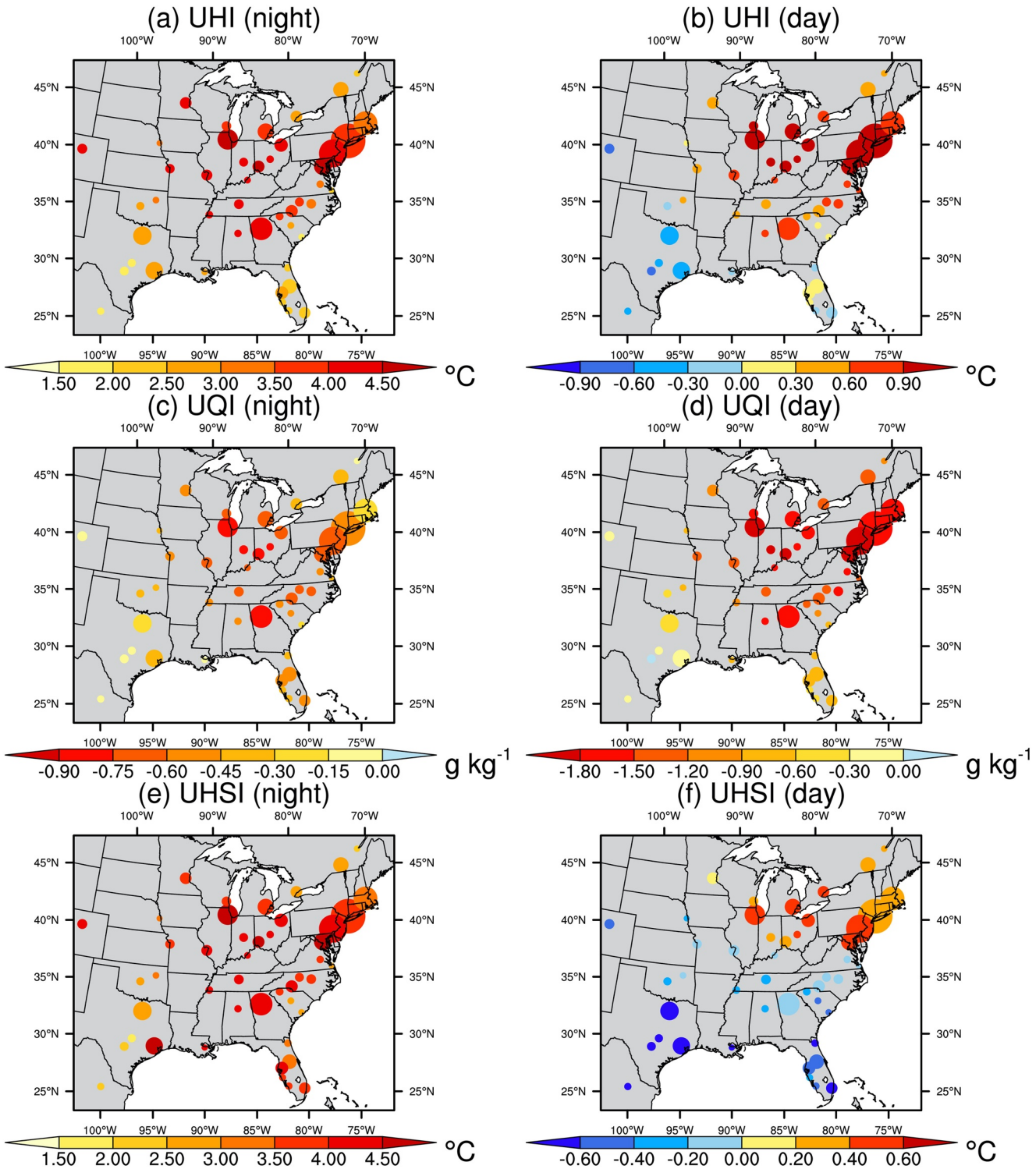

Figure 2. Spatiotemporal variability of simulated 6-year summer mean values of (a) midnight urban heat island (UHI), (b) midday UHI, (c) midnight UQI, (d) midday UQI, (e) midnight urban heat stress intensity (UHSI) and (f) midday UHSI over Eastern US cities. The size of the circle represents the size of the city cluster by population. For the midday and midnight composites, we averaged the hourly outputs between 1100 and 1400 local time and 2100–0200 local time, respectively.

maximum over EUS_{North} (from forest and cropland to urban), followed by EUS_{SE} (from forest, savanna, and cropland to urban) and EUS_{SW} (from savanna and shrub to urban). The differences among the 3 subregions are seen for both midday and midnight periods. The latent heat reduction and sensible heat enhancement are maximum over EUS_{North} and minimum over the EUS_{SE}. Interestingly, over the cities in EUS_{SW} like Houston and Dallas, sensible heat is reduced due to urbanization compared to the background with minimal changes in latent heat flux, which would explain the negative daytime UHI. Reduction in sensible heat and little change in latent heat suggest that the reduction in the UHI is due to the reduction in available energy, which may be related to changes in cloud cover and ground storage. Notably, due to the greater thermal inertia of the urban materials, the mean 6-year UHI over these cities are positive at nighttime despite the negative UHI during daytime.

Figures 2e and 2f depict the urbanization-induced midday and midnight mean UHSI, which depends on changes in both temperature and moisture. As expected from our discussion of UHI and UQI, urbanization leads to larger increase of the UHSI at nighttime (1.9–4.9°C) compared to daytime (−0.8–0.5°C). The impact of UHI seems to dominate the diurnal pattern of UHSI intensity over EUS. Nonetheless, about half of the cities in southern EUS feel more comfortable during daytime (UHSI decreases with background temperature), indicating a non-linear dependence of UHSI on UHI and UQI during daytime. Urbanization increases the air temperature in urban areas, but it also decreases the moisture availability and the peak intensities of these effects are not synchronized during the day.

As UHI and UQI have opposite effect on UHSI, the duration of UHI and UQI during the day has important implications. On average, the duration or number of hours in a day with positive UHI, negative UQI and positive UHSI is ∼15–22 hr day^{-1} (Figures S6a–S6c in Supporting Information S1) over most of the cities in EUS. To better understand this, their diurnal variability is also analyzed (Figures S6d–S6f in Supporting Information S1). While UHI peaks during nighttime, UQI intensities are higher during daytime (Figures S6d–S6e in Supporting Information S1). In southwestern EUS, negative UHI combined with low UQI intensity during the day result in negative UHSI values in daytime (Figure S6f in Supporting Information S1). Thus, differences of the UHSI hours among cities are determined by the net diurnal variability in the intensity of UHI and UQI, which depends on the background climate. Overall, the influence of UHI on UHSI is stronger than the influence of UQI, except for daytime in EUS_{SE}.

5. Sensitivity of UHI, UQI and UHSI to Background Temperature

Here, we examine the sensitivity of UHI, UQI, and UHSI to the ambient air temperature, with a focus on how they vary between hotter and cooler days. Figures 3a and 3b display the linear regression slope between the simulated UHI and the background air temperature for midnight and midday, respectively, for each city cluster. The background temperature is obtained from the NO_URB simulation. A robust positive regression slope between the background temperature and the UHI intensity is notable during nighttime, suggesting that UHI effect tends to be stronger on hotter summer nights. Specifically, the nighttime UHI can rise by 0.1–0.4°C for each degree rise in ambient temperature. However, spatial variations in the magnitudes of the UHI-T slope are also evident, with a pattern opposite to that of UHI (Table S1 in Supporting Information S1). That is, the slope of UHI-T in EUS_{North} (e.g., Chicago, New York) (<0.2) is smaller than that in EUS_{SE} and EUS_{SW} during midnight (mostly >0.2), while the UHI is strongest in EUS_{North}. For example, an enhancement of 4–5°C in background temperature can lead to ∼0.25–1°C rise in UHI values over northern US but ∼1–1.75°C rise in UHI values over the southern US. This suggests that the regional differences in night-time UHI values between southern EUS and northern EUS (i.e., ∼1–1.5°C as seen in Figure 2) diminishes on above normal hot days in EUS.

Figure 3b displays the linear regression slope between the simulated UQI intensity and the corresponding 2-m air temperature for midday. A robust negative regression slope between the background temperature and the UQI intensity is seen across the EUS. This means urban-induced dryness tends to be stronger on hotter days. Specifically, the dryness of mid and large cities can increase by 0.1–0.2 g kg^{-1} $degree^{-1}$ rise in temperature, which is ∼10–20% enhancement (Figure 2d shows a range of ∼0.1–2 g kg^{-1} for the mean UQI values). This enhancement of UQI is the result of a larger rural-urban contrast in LH on hotter days than cooler days as higher VPD on hotter days increases LH in rural area while LH is limited by available water in the urban surface. Spatially, the slopes of UQI-T over the cities located in EUS_{North} are relatively greater than that over cities in the southern EUS. This

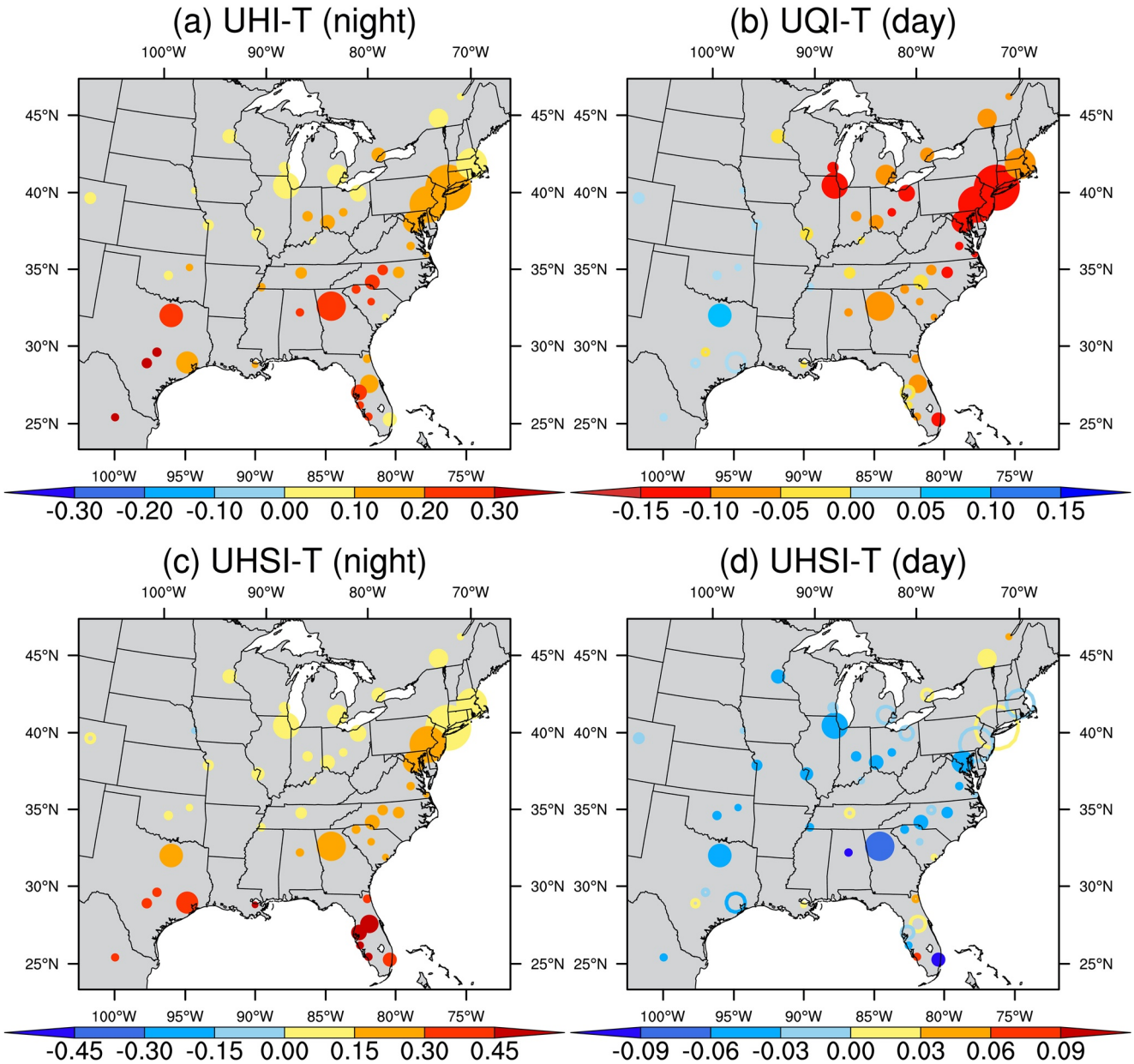

Figure 3. Spatial variability of the slope of regression between background temperature (from NO_URB) and (a) midnight urban heat island, (b) midday UQI, (c) midnight urban heat stress intensity (UHSI) and (d) midday UHSI over Eastern US cities. The size of the circles represent the size of the city cluster and unfilled circles indicate insignificant slope values. The midday and midnight composites are obtained using hourly outputs between 1100 and 1400 local time and 2100–0200 local time, respectively.

is contrary to the spatial pattern of the slopes of UHI-T. The spatial pattern and sign of the UQI-T slopes at night are similar to that during midday, but the intensity is comparatively smaller (Figure not shown).

Figures 3c and 3d shows the regression slopes of UHSI and the background T during midnight and midday, respectively. UHSI and T are positively correlated during nighttime but negatively related during daytime. The enhancement in UHSI with T during nighttime is expected because of the positive UHI-T slope. Interestingly, negative UHSI-T slope values during daytime mean that under heatwave conditions, UHSI does not increase during daytime. This is mainly because the UHI-T slope values during daytime are insignificant (Table S1 in Supporting Information S1), but strong enhancement in UQI (Figure 3b) during hotter days reduces UHSI during daytime. Overall, these findings clearly show the dominant impact of the UHI-T relationship on how UHSI varies

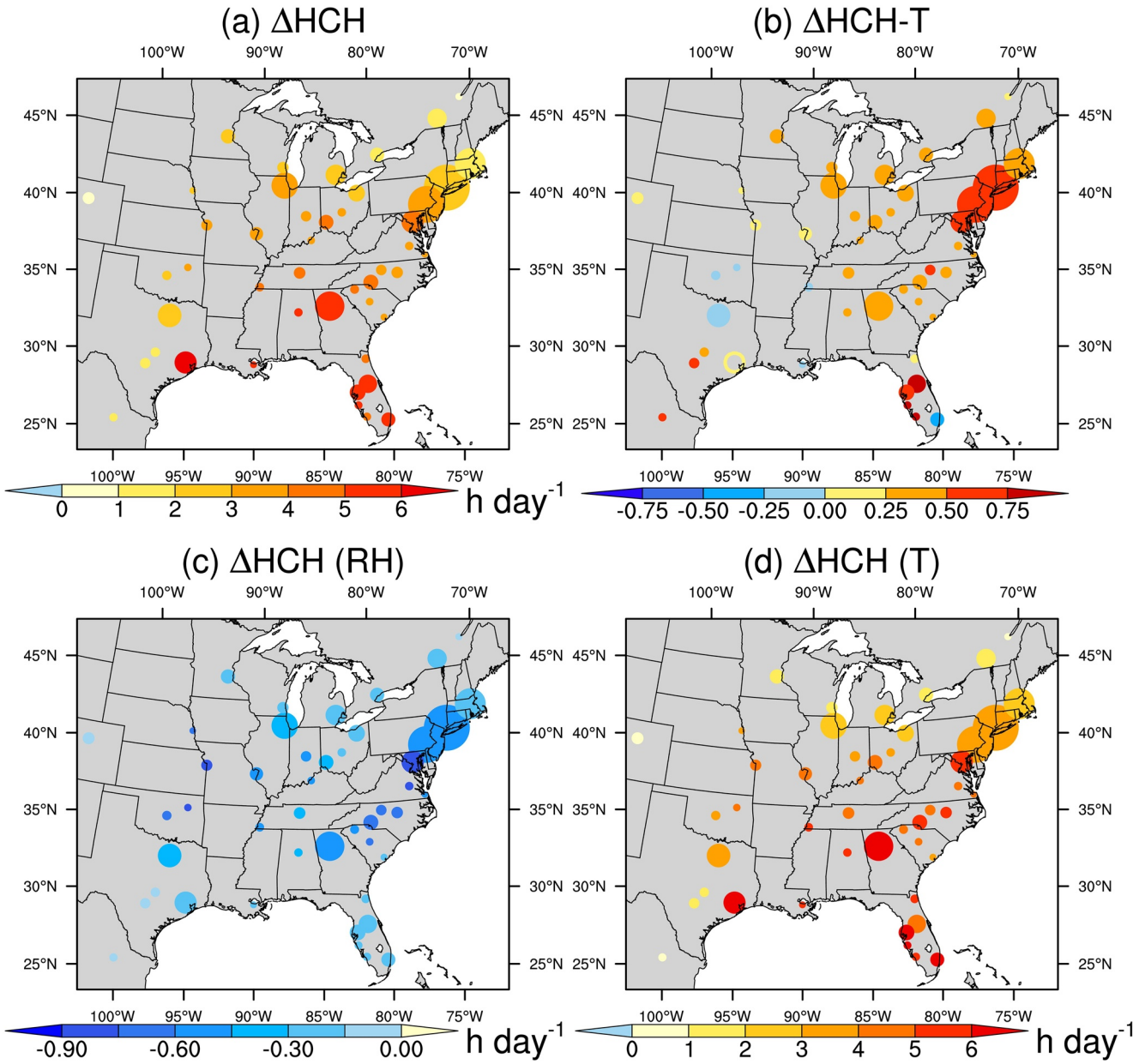

Figure 4. Changes in heat caution hours (ΔHCH) (a) due to urbanization effect and (b) the slope of linear regression between ΔHCH and ambient temperature. Panel (c) illustrates the changes in HCH due only to urban-induced moisture perturbations and (d) only to urban-induced temperature changes.

with the background temperature. The spatial variations in the UHSI-T slope during nighttime follow that of the UHI-T slope, that is, larger slope over EUS_{SE} and EUS_{SW} compared to EUS_{North}. Consequently, for each degree rise in the background temperature, UHSI enhancement is greater (~10%) in the southern cities (Figures 3c and 3d) than the northern cities (Table S1 in Supporting Information S1).

6. Heat Caution Hours

To quantify how urbanization induced heat stress impacts public health, we estimate ΔHCH in a day (i.e., change in the number of hours when HI ≥ 27°C) based on the model simulations. The HCH increases by 2–7 hr day^{-1} due to urbanization (Figure 4a). Interestingly, the largest enhancements are seen over cities in EUS_{SE} (4–7 hr day^{-1}). Cities in EUS_{North} and EUS_{SW} can see HCH enhancements of 2–4 hr day^{-1}. Under hotter conditions, HCH tends

to further increase by ~0.25–0.75 hr day^{-1} degree^{-1} rise In background temperature, mainly over EUS_{North} and EUS_{SE} (Figure 4b). But the impact of urbanization on HCH is mostly insignificant over cities in EUS_{SW}.

To better understand the urbanization-induced changes in HCH, we isolate the impact of UHI and UQI on ΔHCH based on Equations 4 and 5, respectively. As expected, changes in HCH due to temperature and moisture show different signs, and in term of the magnitude, temperature effects are 3–5 times greater than that due to moisture (Figures 4c and 4d). Through changes in moisture, urbanization has a negative effect on ΔHCH for ~0.3–0.6 hr day^{-1} (Figure 4c). But, temperature changes due to urbanization have a positive effect on ΔHCH by ~3–7 hr day^{-1} (Figure 4d). Thus, the variabilities in UHSI and ΔHCH are mainly dominated by the temperature enhancement associated with urbanization (Figure 4d). Moreover, the spatial distribution of the 6-year mean ΔHCH purely due to temperature changes matches very well with the spatial pattern of the urbanization-induced ΔHCH (Figure 4a). However, there are subtle evidence of a strong influence of background moisture on the spatial variability of ΔHCH. Among the EUS_{SE} cities, the spatial pattern of the ΔHCH-T slope (Figure 4b) shows relatively larger slope over cities near the coast. For example, HCH rises by ~0.75 hr day^{-1} degree^{-1} rise in background temperature for cities in Florida but only ~0.5 hr day^{-1} degree^{-1} rise in Atlanta.

7. Discussions and Summary

For cities in EUS, peak UHI has a range of ~2.5–4°C and the corresponding peak urban-induced dryness has a range of ~0.5–2 g kg^{-1}. While the UHI peaks during nighttime, the diurnal peak of UQI occurs during daytime. UHSI is strongly enhanced by increases in the background temperature. Quantitatively, the urban-induced heat stress exposure can increase by ~3–5 hr day^{-1} over EUS cities. In rural areas, the surface energy partitioning shifts toward greater evaporative fraction under hotter conditions, but in urban areas, this shift is suppressed by the lack of vegetation and surface moisture. This mechanism largely explains the positive UHI-T (and thus the positive UHSI-T) relationship. In addition to enhancing the UHSI, increases in background temperature also lengthen the duration of heat caution hours. Therefore, urbanization affects both the magnitude and duration of heat stress. Importantly, the UHSI-T relationship has strong spatial-diurnal variability, with the steepest enhancement in UHSI per degree rise in temperature simulated over EUS_{SE} during nighttime. Our study highlights the importance of considering both UHI and UQI for understanding the diurnal variability in urban heat stress over EUS. As UHSI is enhanced under hotter and wetter conditions, enhancement in the urban-induced dryness can partially negate the rise in daytime UHSI during heatwaves.

Understanding the impacts of urbanization is increasingly relevant as global and regional urban extent increases with time. Traditionally, there are two types of observational analysis of urban-induced thermal changes–one in which urbanization effects are estimated based on the differences in temperature distribution over urban and rural sites and another based on comparison of the trends of temperature observed over urban and rural sites. The first approach provides an understanding of the spatial characteristics of UHI specific to the contemporary phase of urban expansion and the approach is similar to estimating $UHI_{surface}$ using MODIS data (Figure 1a). The second approach represents the cumulative effect of urbanization on temperature, which is influenced by the sensitivity of UHI to climate variability. Recently, Krayenhoff et al. (2018) and Guo et al. (2019) highlighted the non-linear (or even opposing) interactions between urbanization and global-warming induced future temperature changes. Hence sensitivity of UHI, UQI, and UHSI to background temperature variations in the current climate should not be interpreted as how the impacts of urbanization respond to future global warming. Furthermore, our approach of comparing model simulations with and without the urban grids is different from the two approaches used in observational analysis. Thus, the simulated magnitudes of UHI/UQI and UHSI are expected to show differences from estimations by satellites or other previous observational studies.

Besides differences in the analysis methods, uncertainties in the physical parameterizations, the limitations of night-light based urban definitions and representation of sub-grid land processes could also contribute to biases in theo simulations. The well-known dry and warm biases in central and eastern US associated with biases in the large-scale circulation may also influence the simulation of urbanization effects. As the role of UQI is shown to be significant in understanding the UHSI-T relationship, the lack of detailed bio-physical and plant physiological processes in our model could also contribute to some uncertainties.

Despite the model biases mentioned above, our analysis builds a robust baseline for understanding the sensitivity of UHSI to background temperature in US. As urban-induced moisture and temperature changes can affect UHSI

differently at different times of the day, which also depend on the background climate, future mitigation strategies should be informed by detailed and city-specific analysis and modeling.

Data Availability Statement

The scripts for Figures, model data, code and scripts are available at https://portal.nersc.gov/project/m2645/pnnl/GRL2021_UHI/

Acknowledgments
This study is supported by the Office of Science of the US Department of Energy Biological and Environmental Research as part of the Regional and Global Model Analysis program area. The Pacific Northwest National Laboratory is operated by Battelle for the US Department of Energy under Contract DE-AC05-76RLO1830. CS acknowledges research support from MHRD, India under Institute of Eminence (pIOE) funding project number SB20210835CEMHRD00850.

References

Basara, J. B., Hall, P. K., Schroeder, A. J., Illston, B. G., & Nemunaitis, K. L. (2008). Diurnal cycle of the Oklahoma City urban heat island. *Journal of Geophysical Research Atmospheres*, *113*(20), D20109. https://doi.org/10.1029/2008JD010311

Chakraborty, T., Hsu, A., Manya, D., & Sheriff, G. (2020). A spatially explicit surface urban heat island database for the United States: Characterization, uncertainties, and possible applications. *ISPRS Journal of Photogrammetry and Remote Sensing*, *168*, 74–88. https://doi.org/10.1016/j.isprsjprs.2020.07.021

Chakraborty, T., Sarangi, C., & Tripathi, S. N. (2017). Understanding diurnality and inter-seasonality of a sub-tropical urban heat island. *Boundary-Layer Meteorology*, *163*(2), 287–309. https://doi.org/10.1007/s10546-016-0223-0

Chakraborty, T. C., Sarangi, C., & Lee, X. (2021). Reduction in human activity can enhance the urban heat island: Insights from the COVID-19 lockdown. *Environmental Research Letters*, *16*(5), 054060. https://doi.org/10.1088/1748-9326/abef8e

Chen, F., & Dudhia, J. (2001). Coupling an advanced land surface–Hydrology model with the Penn State–NCAR MM5 modeling system. Part I: Model implementation and sensitivity. *Monthly Weather Review*, *129*(4). https://doi.org/10.1175/1520-0493(2001)129<0569:caalsh>2.0.co;2

Chen, F., Yang, X., & Zhu, W. (2014). WRF simulations of urban heat island under hot-weather synoptic conditions: The case study of Hangzhou City, China. *Atmospheric Research*, *138*, 364–377. https://doi.org/10.1016/j.atmosres.2013.12.005

Chew, L. W., Liu, X., Li, X. X., & Norford, L. K. (2021). Interaction between heat wave and urban heat island: A case study in a tropical coastal city, Singapore. *Atmospheric Research*, *247*, 105134. https://doi.org/10.1016/j.atmosres.2020.105134

Chou, M.-D., & Suarez, M. J. (1994). *An efficient thermal infrared radiation parameterization for use in general circulation models*.

Daly, C., Smithy, J. W., Smith, J. I., & McKane, R. B. (2007). High-resolution spatial modeling of daily weather elements for a catchment in the Oregon Cascade Mountains, United States. *Journal of Applied Meteorology and Climatology*, *46*(10), 1565–1586. https://doi.org/10.1175/jam2548.1

Du, H., Ai, J., Cai, Y., Jiang, H., & Liu, P. (2019). Combined effects of the surface urban heat island with landscape composition and configuration based on remote sensing: A case study of Shanghai, China. *Sustainability*, *11*(10), 2890. https://doi.org/10.3390/su11102890

Estrada, F., Botzen, W. J. W., & Tol, R. S. J. (2017). A global economic assessment of city policies to reduce climate change impacts. *Nature Climate Change*, *7*(6), 403–406. https://doi.org/10.1038/nclimate3301

Fischer, E. M., Oleson, K. W., & Lawrence, D. M. (2012). Contrasting urban and rural heat stress responses to climate change. *Geophysical Research Letters*, *39*(3), L03705. https://doi.org/10.1029/2011GL050576

Frumkin, H. (2002). Urban sprawl and public health. *Public Health Reports*, *117*(3). https://doi.org/10.1016/s0033-3549(04)50155-3

Guo, E., Zhang, J., Wang, Y., Quan, L., Zhang, R., Zhang, F., & Zhou, M. (2019). Spatiotemporal variations of extreme climate events in Northeast China during 1960–2014. *Ecological Indicators*, *96*, 669–683. https://doi.org/10.1016/j.ecolind.2018.09.034

Hao, L., Huang, X., Qin, M., Liu, Y., Li, W., & Sun, G. (2018). Ecohydrological processes explain urban dry island effects in a wet region, southern China. *Water Resources Research*, *54*(9), 6757–6771. https://doi.org/10.1029/2018WR023002

Hong, S. Y., & Lim, J. O. J. (2006). The WRF single-moment 6-class microphysics scheme (WSM6). *Asia-Pacific Journal of Atmospheric Sciences*, *42*(2), 129–151

Janjić, Z. I. (1994). The step-mountain eta coordinate model: Further developments of the convection, viscous sublayer, and turbulence closure schemes. *Monthly Weather Review*, *122*(5), 2. https://doi.org/10.1175/1520-0493

Janjić, Z. I. (2001). *Nonsingular implementation of the mellor-yamada level 2.5 scheme in the NCEP meso model*.

Jia, L., Ma, Q., Du, C., Hu, G., & Shang, C. (2020). Rapid urbanization in a mountainous landscape: Patterns, drivers, and planning implications. *Landscape Ecology*, *35*, 2449–2469. https://doi.org/10.1007/s10980-020-01056-y

Kalnay, E., & Cai, M. (2003). Impact of urbanization and land-use change on climate. *Nature*, *423*(6939), 528–531. https://doi.org/10.1038/nature01675

Katavoutas, G., & Founda, D. (2019). Response of urban heat stress to heat waves in Athens (1960–2017). *Atmosphere*, *10*(9), 483. https://doi.org/10.3390/atmos10090483

Krayenhoff, E. S., Moustaoui, M., Broadbent, A. M., Gupta, V., & Georgescu, M. (2018). Diurnal interaction between urban expansion, climate change and adaptation in US cities. *Nature Climate Change*, *8*(12), 1097–1103. https://doi.org/10.1038/s41558-018-0320-9

Kusaka, H., & Kimura, F. (2004). Coupling a single-layer urban canopy model with a simple atmospheric model: Impact on urban heat island simulation for an idealized case. *Journal of the Meteorological Society of Japan*, *82*(Issue 1). https://doi.org/10.2151/jmsj.82.67

Kusaka, H., Kondo, H., Kikegawa, Y., & Kimura, F. (2001). *A simple single-layer urban canopy model for atmospheric models: Comparison with multi-layer and slab models*.

Laaidi, K., Zeghnoun, A., Dousset, B., Bretin, P., Vandentorren, S., Giraudet, E., & Beaudeau, P. (2012). The impact of heat islands on mortality in Paris during the August 2003 heat wave. *Environmental Health Perspectives*, *120*(2), 254–259. https://doi.org/10.1289/ehp.1103532

Lee, S. H., McKeen, S. A., & Sailor, D. J. (2014). A regression approach for estimation of anthropogenic heat flux based on a bottom-up air pollutant emission database. *Atmospheric Environment*, *95*, 629–633. https://doi.org/10.1016/j.atmosenv.2014.07.009

Li, D., & Bou-Zeid, E. (2013). Synergistic Interactions between Urban Heat Islands and Heat Waves: The Impact in Cities Is Larger than the Sum of Its Parts. *Journal of Applied Meteorology and Climatology*, *52*(9). https://doi.org/10.1175/jamc-d-13-02.1

Li, D., & Bou-Zeid, E. (2014). Quality and sensitivity of high-resolution numerical simulation of urban heat islands. *Environmental Research Letters*, *9*(5), 055001. https://doi.org/10.1088/1748-9326/9/5/055001

Li, D., Sun, T., Liu, M., Yang, L., Wang, L., & Gao, Z. (2015). Contrasting responses of urban and rural surface energy budgets to heat waves explain synergies between urban heat islands and heat waves. *Environmental Research Letters*, *10*(5), 054009. https://doi.org/10.1088/1748-9326/10/5/054009

Lin, Y., Dong, W., Zhang, M., Xie, Y., Xue, W., Huang, J., & Luo, Y. (2017). Causes of model dry and warm bias over central U.S. and impact on climate projections. *Nature Communications*, *8*(1). https://doi.org/10.1038/s41467-017-01040-2

Ma, H. Y., Klein, S. A., Xie, S., Zhang, C., Tang, S., Tang, Q., et al. (2018). CAUSES: On the role of surface energy budget errors to the warm surface air temperature error over the Central United States. *Journal of Geophysical Research: Atmospheres*, *123*(5), 2888–2909. https://doi.org/10.1002/2017JD027194

Manoli, G., Fatichi, S., Bou-Zeid, E., & Katul, G. G. (2020). Seasonal hysteresis of surface urban heat islands. *Proceedings of the National Academy of Sciences*, *117*(13), 7082–7089. https://doi.org/10.1073/pnas.1917554117

Mesinger, F., DiMego, G., Kalnay, E., Mitchell, K., Shafran, P. C., Ebisuzaki, W., et al. (2006). North American regional reanalysis. *Bulletin of the American Meteorological Society*, *87*(3), 343–360. https://doi.org/10.1175/BAMS-87-3-343

Mlawer, E. J., Taubman, S. J., Brown, P. D., Iacono, M. J., & Clough, S. A. (1997). Radiative transfer for inhomogeneous atmospheres: RRTM, a validated correlated-k model for the longwave. *Journal of Geophysical Research*, *102*(14), 16663–16682. https://doi.org/10.1029/97jd00237

Morcrette, C. J., Van Weverberg, K., Ma, H. Y., Ahlgrimm, M., Bazile, E., Berg, L. K., et al. (2018). Introduction to CAUSES: Description of weather and climate models and their near-surface temperature errors in 5 day hindcasts near the Southern Great Plains. *Journal of Geophysical Research: Atmospheres*, *123*(5), 2655–2683. https://doi.org/10.1002/2017JD027199

Oke, T. R., & Cleugh, H. A. (1987). Urban heat storage derived as energy balance residuals. *Boundary-Layer Meteorology*, *39*(3), 233–245. https://doi.org/10.1007/BF00116120

Oke, T. R., Johnson, G. T., Steyn, D. G., & Watson, I. D. (1991). Simulation of surface urban heat islands under "ideal" conditions at night part 2: Diagnosis of causation. *Boundary-Layer Meteorology*, *56*(4), 339–358. https://doi.org/10.1007/BF00119211

Qian, Y., Yang, Z., Feng, Z., Liu, Y., Gustafson, W. I., Berg, L. K., et al. (2020). Neglecting irrigation contributes to the simulated summertime warm-and-dry bias in the central United States. *Npj Climate and Atmospheric Science*, *3*(1). https://doi.org/10.1038/s41612-020-00135-w

Ramamurthy, P., & Bou-Zeid, E. (2017). Heatwaves and urban heat islands: A comparative analysis of multiple cities. *Journal of Geophysical Research*, *122*(1), 168–178. https://doi.org/10.1002/2016JD025357

Ritchie, H., & Max, R. (2018). *Urbanization. Our World in data*. https://ourworldindata.org/urbanization

Schatz, J., & Kucharik, C. J. (2015). Urban climate effects on extreme temperatures in Madison, Wisconsin, USA. *Environmental Research Letters*, *10*(9), 094024. https://doi.org/10.1088/1748-9326/10/9/094024

Scott, A. A., Waugh, D. W., & Zaitchik, B. F. (2018). Reduced Urban Heat Island intensity under warmer conditions. *Environmental Research Letters*, *13*(6), 064003. https://doi.org/10.1088/1748-9326/aabd6c

Sherwood, S. C., & Huber, M. (2010). An adaptability limit to climate change due to heat stress. *Proceedings of the National Academy of Sciences*, *107*(21), 9552–9555. https://doi.org/10.1073/pnas.0913352107

Skamarock, W. C., & Klemp, J. B. (2008). A time-split nonhydrostatic atmospheric model for weather research and forecasting applications. *Journal of Computational Physics*, *227*(7), 3465–3485. https://doi.org/10.1016/j.jcp.2007.01.037

Steadman, R. G. (1971). Indices of windchill of clothed persons. *Journal of Applied Meteorology*, *10*(4). https://doi.org/10.1175/1520-0450(1971)010<0674:iowocp>2.0.co;2

Tan, J., Zheng, Y., Tang, X., Guo, C., Li, L., Song, G., et al. (2010). The urban heat island and its impact on heat waves and human health in Shanghai. *International Journal of Biometeorology*, *54*(1), 75–84. https://doi.org/10.1007/s00484-009-0256-x

Tewari, M., Yang, J., Kusaka, H., Salamanca, F., Watson, C., & Treinish, L. (2019). Interaction of urban heat islands and heat waves under current and future climate conditions and their mitigation using green and cool roofs in New York City and Phoenix, Arizona. *Environmental Research Letters*, *14*(3), 034002. https://doi.org/10.1088/1748-9326/aaf431

Thompson, G., Field, P. R., Rasmussen, R. M., & Hall, W. D. (2008). Explicit forecasts of winter precipitation using an improved bulk microphysics scheme. Part II: Implementation of a new snow parameterization. *Monthly Weather Review*, *136*(12), 5095–5115. https://doi.org/10.1175/2008MWR2387.1

Varquez, A. C. G., & Kanda, M. (2018). Global urban climatology: A meta-analysis of air temperature trends (1960–2009). *Npj Climate and Atmospheric Science*, *1*(1). https://doi.org/10.1038/s41612-018-0042-8

Wang, X., & Gong, Y. (2010). The impact of an urban dry island on the summer heat wave and sultry weather in Beijing City. *Chinese Science Bulletin*, *55*(16), 1657–1661. https://doi.org/10.1007/s11434-010-3088-5

Wouters, H., De Ridder, K., Poelmans, L., Willems, P., Brouwers, J., Hosseinzadehtalaei, P., et al. (2017). Heat stress increase under climate change twice as large in cities as in rural areas: A study for a densely populated midlatitude maritime region. *Geophysical Research Letters*, *44*(17), 8997–9007. https://doi.org/10.1002/2017GL074889

Yang, B., Yang, X., Leung, L. R., Zhong, S., Qian, Y., Zhao, C., et al. (2019). Modeling the impacts of urbanization on summer thermal comfort: The role of urban land use and anthropogenic heat. *Journal of Geophysical Research: Atmospheres*, *124*(13), 6681–6697. https://doi.org/10.1029/2018JD029829

Zhao, L., Oppenheimer, M., Zhu, Q., Baldwin, J. W., Ebi, K. L., Bou-Zeid, E., et al. (2018). Interactions between urban heat islands and heat waves. *Environmental Research Letters*, *13*(3), 034003. https://doi.org/10.1088/1748-9326/aa9f73